Synergy between Confined Cobalt Centers and Oxygen Defects on α-Fe 2 O 3 Platelets for Efficient Photocatalytic CO 2 Reduction

Synergy between Confined Cobalt Centers and Oxygen Defects on α-Fe_2O_3 Platelets for Efficient Photocatalytic CO_2 Reduction

Gaoliang Yang, Yunxiang Li, Qi Wang, Xusheng Wang, Shouwei Zuo, Huabin Zhang, Xiaohui Ren, Yu He, Fumihiko Ichihara and Jinhua Ye**

Dr. G. Yang, Q. Wang, X. Ren, Prof. J. Ye

Graduate School of Chemical Science and Engineering, Hokkaido University, Sapporo 060-0814, Japan

E-mail: Jinhua.YE@nims.go.jp

Dr. G. Yang, Dr. Y. Li, Q. Wang, Dr. X. Wang, X. Ren, Dr. Y. He, Dr. F. Ichihara, Prof. J. Ye

International Center for Materials Nanoarchitectonics (WPI-MANA), National Institutes for Materials Science (NIMS), 1-1 Namiki, Tsukuba, Ibaraki 305-0044, Japan

Prof. J. Ye

TJU-NIMS International Collaboration Laboratory, School of Materials Science and Engineering, Tianjin University, Tianjin 300072, P. R. China

Dr. X. Wang

Institute of Functional Porous Materials, School of Materials Science and Engineering, Zhejiang Sci-Tech University, Hangzhou 310018, China

E-mail: xswang@zstu.edu.cn

Dr. S. Zuo

This article has been accepted for publication and undergone full peer review but has not been through the copyediting, typesetting, pagination and proofreading process, which may lead to differences between this version and the Version of Record. Please cite this article as doi: 10.1002/solr.202100833.

Beijing Synchrotron Radiation Facility, Institute of High Energy Physics, Chinese Academy of Sciences, Beijing 100049, China

Dr. H. Zhang

KAUST Catalysis Center, Physical Sciences and Engineering Division, King Abdullah University of Science and Technology, Thuwal, 23955-6900, Saudi Arabia

Keywords: (confined cobalt centers, oxygen defects, synergetic effects, CO_2 photoreduction)

Abstract: Cocatalysts loading is one of the most effective strategies for boosting CO_2 photoreduction. Thus, constructing robust active sites with a specific chemical environment on the cocatalyst to selectively convert CO_2 to chemical fuels is highly desirable, but remains challenging. Herein, α-Fe_2O_3 platelets modulated with confined Co centers and oxygen defects are designed as efficient cocatalysts for photocatalytic CO_2 reduction with superior activity and CO selectivity. The highly dispersed Co centers can proceed the catalytic processes efficiently as the reaction sites, while the oxygen vacancies enable to enhance the CO_2 adsorption/activation. After integrating together, the oxygen defects provide vigorous assistances to promote the catalytic activity of confined Co sites, leading to facilitated charge transfer and reduced energy barriers for CO_2 photoreduction. As a result, the optimized catalyst achieves a CO generation rate of 37.8 μmol h^{-1} with an impressive selectivity of 80.2%, as well as remarkable durability for photocatalytic CO_2 reduction. This work demonstrates new insights of developing robust catalysts by controlling confined active sites together with defects engineering for efficient photocatalytic CO_2 conversion.

1. Introduction

Solar-driven CO_2 conversion into valuable chemical products has attracted tremendous attentions due to the great potential in managing the global carbon balance and addressing the energy crisis.[1-3] Due to the chemical stability of CO_2 molecules, the sluggish kinetics of charge transfer processes and the fierce competition with water splitting reactions, considerable barriers still exist in both thermodynamics and kinetics to achieve highly efficient CO_2 activation and conversion.[4-6] Therefore, constructing advanced

photocatalytic systems for CO_2 reduction with superior conversion efficiency and selectivity for desirable products still remain a great challenge.[7-9]

Notable, photocatalytic CO_2 reduction can be significantly ignited by cocatalysts via reducing the energy barriers to the targeted products and facilitating the charge transfer processes.[10-12] Recently, transition-metal based cocatalysts, such as the oxide, sulfide and phosphide, have been intensively explored as alternatives for noble-metal catalysts for CO_2 photoreduction due to the excellent intrinsic catalytic activity and low cost.[13-16] However, because of the limited active sites that are accessible to the reactants, these kinds of cocatalysts usually exhibit rather low atom utilization efficiency.[17-19] Thus, developing robust active sites on cocatalysts with high accessibility is crucial for efficient CO_2 conversion.[2, 20] As a nascent research field, downsizing the cocatalysts to clusters or even atomic sites provides an effective approach to boost the photocatalytic activity with maximized utilization for active sites and extraordinary catalytic properties.[21-23] Generally, the atomic metal sites are immobilized on appropriate support materials to realize unique electronic structures and maximum reactive centers.[24, 25] Therefore, modulation over the support materials to promote the catalytic activity of active sites on the cocatalysts is significantly important for CO_2 photoreduction and needs to be systematically investigated.

To completely exploit the potential of single-atom based cocatalysts for photocatalytic reactions, two critical issues should be fulfilled: i) efficient transfer of photogenerated charge carriers to the atomical reaction sites; ii) sufficient CO_2 adsorption onto the catalysts. Due to the strong interaction between the atomical active sites and the support, photogenerated electrons can be facilitated to transfer from photosensitizer to the highly dispersed catalytic sites.[26, 27] Therefore, the adsorption/activation of CO_2 molecules on the catalysts are critical for efficient photocatalytic reaction. In recent years, oxygen defects engineering has been reported as an effective strategy to promote the CO_2 conversion with enhanced CO_2 adsorption/activation.[28-30] The oxygen vacancies can anchor the CO_2 molecules with stable configurations and activate the C=O bonds more easily due to the modified coordination environment and delocalized charge distribution.[31, 32] However, the performance of defects-engineered catalyst is moderate due to the lack of robust active sites. Therefore, it is anticipated to utilize the defects engineering as assistances to further boost the catalytic activity of the cocatalysts, which are expected to achieve favorable CO_2 adsorption/activation and reduced energy barriers for CO_2 photoreduction.

Owing to the intrinsic properties of α-Fe_2O_3, it is highly feasible to implant metal dopants and introduce oxygen defects onto the α-Fe_2O_3, which can be utilized as a prototype to investigate the synergetic effect of atomic metal sites and oxygen vacancies for photocatalytic CO_2 reduction. Thus, in this study, well dispersed Co sites are confined on the α-Fe_2O_3 platelets and abundant oxygen defects can be generated simultaneously with the Co decoration. Notably, the existence of oxygen defects can assist to improve the

catalytic activity of confined Co centers for CO_2 photoreduction due to the enhanced CO_2 adsorption and facilitated charge transfer. Benefiting from the synergy of confined Co centers and oxygen defects, the optimized 1%Co-α-Fe_2O_3 delivers outstanding photocatalytic performance for CO_2 conversion, with a CO generation rate of 37.8 μmol h^{-1} and an impressive CO selectivity of 80.2%.

2. Results and Discussion

Figure 1a presents the scanning electron microscope (SEM) image of as-prepared 1%Co-α-Fe_2O_3, which displays similar morphology as the bare α-Fe_2O_3 in Figure S1. Both of the α-Fe_2O_3 and 1%Co-α-Fe_2O_3 exhibit platelet-like shapes with a homogenous planar size of ~150 nm (Figure S2), signifying that the Co decoration would not change the morphology of α-Fe_2O_3, which is further verified by the SEM images with different amounts of Co on α-Fe_2O_3 (Figure S4). To clarify the detailed structure of 1%Co-α-Fe_2O_3, transmission electron microscopy (TEM) was conducted. Similarly, the TEM image in Figure 1b validates the platelet-like morphology of 1%Co-α-Fe_2O_3. The high-resolution TEM (HRTEM) image demonstrates the well-crystallized properties of 1%Co-α-Fe_2O_3. No obvious nanoparticles or clusters are observed on 1%Co-α-Fe_2O_3 from the HRTEM image (Figure 1c), which is further confirmed by the typical selected area electron diffraction (SAED) pattern of monocrystalline α-Fe_2O_3 (inset in Figure 1c). In addition, no distinct difference can be detected from the bright spots (in Figure 1d) corresponding to metal sites in 1%Co-α-Fe_2O_3, probably due to the relatively low contrast between Fe and Co atoms.[33, 34] The measured interplanar distance of 0.25 nm in Figure 1d is corresponding to the (110) crystal plane of α-Fe_2O_3, which is consistent with the SAED pattern in Figure 1c, indicating that no additional phases would be formed on α-Fe_2O_3 after Co decoration. However, the elemental mapping by TEM-EDS (energy-dispersive X-ray spectroscopy) (Figure 1e) evidences the existence of Co species across the entire architecture of α-Fe_2O_3, indicating the high dispersion of confined Co centers on the surface of α-Fe_2O_3 platelets. The loading amount of Co is determined to be ~0.42 wt% for the 1%Co-α-Fe_2O_3 (Figure S5) by inductively coupled plasma atomic emission spectrometry (ICP-AES). The X-ray diffraction (XRD) pattern of 1%Co-α-Fe_2O_3 is similar with the pure α-Fe_2O_3 (Figure S3), signifying that the decorated Co in 1%Co-α-Fe_2O_3 would not alter the crystal structure of the α-Fe_2O_3. By tuning the Co amounts in the precursors, a series of α-Fe_2O_3 platelets with different mass loading of Co can be obtained. With the increasing of Co amount, nanoparticles can be gradually formed and deposited on the surface of α-Fe_2O_3 platelets (Figure S4). In order to verify the structure and composition of the nanoparticles with high mass loading of Co (taking 4% as the example), TEM images and SAED patterns were presented in Figure S6 and Figure S7b. Plenty of nanoparticles with different sizes (ranging from several nanometers to several tens nanometers), which are identified as CoO_x according to the measurements of interplanar distances and SAED patterns,[35, 36] can be observed on 4%Co-

α-Fe_2O_3. Based on the above results and analysis in Figure S7, it is reasonable to deduced that the Co atoms would be confined in the lattice of the α-Fe_2O_3 when the loading amount is low (1%). However, when further increasing the Co amount, the Co atoms are inclined to aggregate and finally form the CoO_x nanoparticles on the surface of α-Fe_2O_3 (2%~4%).

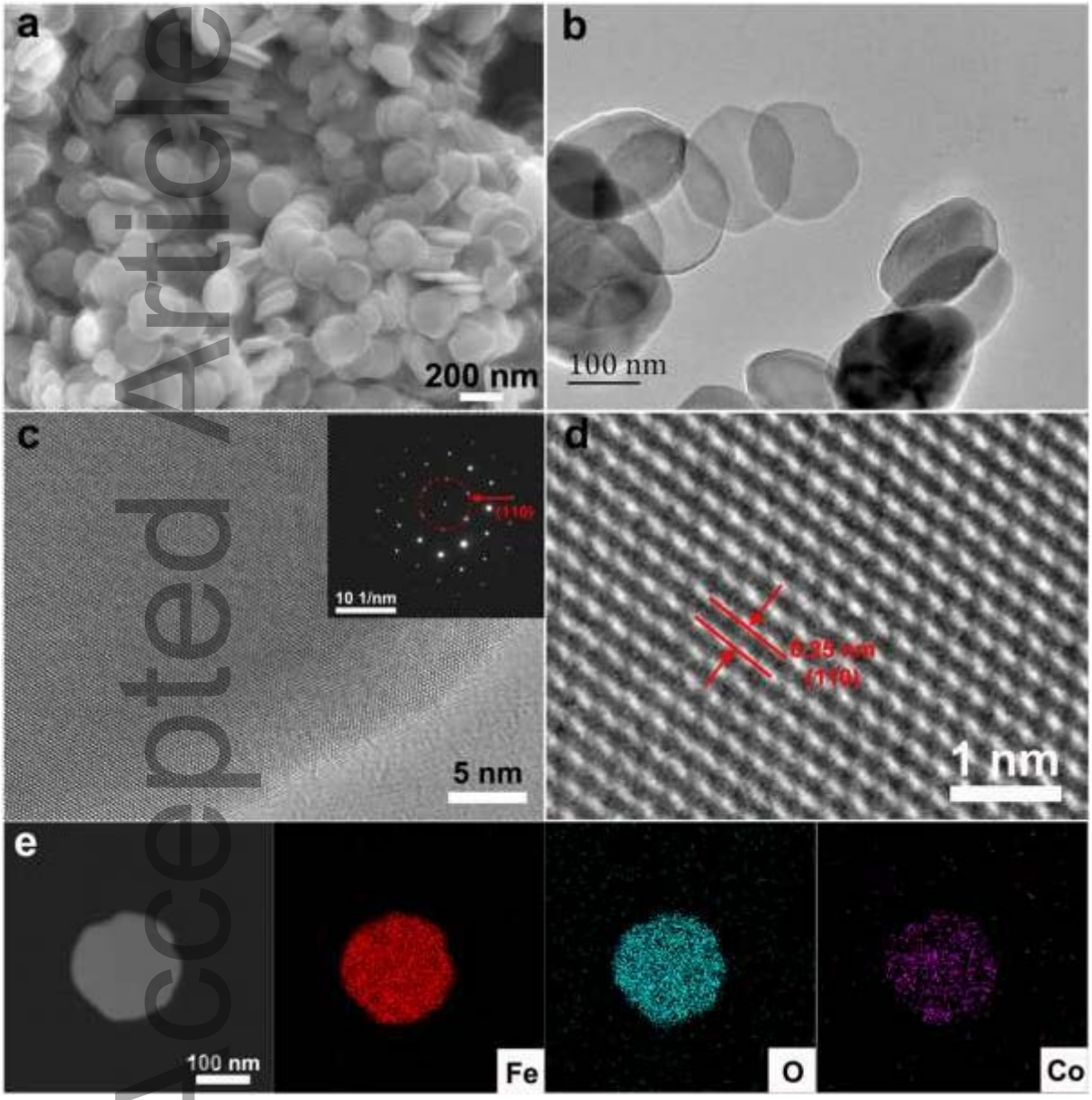

Figure 1. Morphology characterizations of 1%Co-α-Fe_2O_3. a) SEM image; b) TEM image; c-d) HRTEM images (inset is the SAED pattern); e) EDS elemental mapping images refer to the signals of Fe, O and Co, respectively.

In order to confirm the distribution of Co sites on the surface of α-Fe_2O_3, the local structure of Co species was investigated by the X-ray absorption fine structure (XAFS) measurement. Unfortunately, due to the adjacent atomic numbers of Co and Fe elements, it is considerably difficult to distinguish the Co element

from α-Fe_2O_3 support via the XAFS investigation, especially when the loading content of Co is quite low comparing with the Fe species. The quality of the XAFS spectrum for 1%Co-α-Fe_2O_3 is not good enough for quantitative analysis. As such, in order to obtain a valid spectrum for the Co sites, XAFS measurement was conducted on the 4%Co-α-Fe_2O_3 with high Co loading amount. As shown in Figure 2a, the Co K-edge X-ray absorption near-edge structure (XANES) spectrum of 4%Co-α-Fe_2O_3 exhibits a similar shape as the three referenced cobalt oxides (CoO, Co_3O_4 and Co_2O_3), indicating that the composition of the Co species in 4%Co-α-Fe_2O_3 is CoO_x, which is consistent with the TEM and SEAD results. Interestingly, an obvious negative shift of the peaks in 4%Co-α-Fe_2O_3 can be observed compared with all the referenced cobalt oxides, signifying the electron transfer from α-Fe_2O_3 support to the Co sites.[37] Therefore, the XAFS results confirm the formation of CoO_x with the high loading amount of Co. More importantly, it also verifies the facilitated charge transfer between the Co sites and α-Fe_2O_3 support, which is crucial to achieve efficient photocatalytic CO_2 reduction.

The oxygen defects on α-Fe_2O_3 platelets were illustrated by the X-ray photoelectron spectroscopy (XPS) measurement. As displayed in the O *1s* XPS spectra (Figure 2b), two different peaks can be observed at ~529.6 eV and ~531.8 eV, which are corresponding to the lattice oxygen (O_L) and the O atoms in the vicinity of oxygen vacancies (O_V), respectively.[38, 39] As clearly obtained from the calculated integral-area ratios, the area ratio of the O_V peak for 1%Co-α-Fe_2O_3 (45.9%) is much larger than that of the bare α-Fe_2O_3 (30.3%), indicating the formation of oxygen defects after Co decoration on α-Fe_2O_3.[33] The oxygen vacancies were also identified by the electron paramagnetic resonance (EPR) spectra. As shown in Figure S8, similar axial signals can be found both in α-Fe_2O_3 and 1%Co-α-Fe_2O_3， which are attributed to the surface electron trapped on oxygen vacancies (g=2.0005).[40] The much higher intensity of EPR signal at g=2.0005 for 1%Co-α-Fe_2O_3 indicates that the concentration of oxygen vacancies is greatly enhanced after decorating Co on α-Fe_2O_3.[41] Furthermore, as obtained from the UV-vis diffuse reflectance spectra in Figure S9a, new decaying absorption tails are presented between 600 and 750 nm due to the existence of abundant defects on Co decorated α-Fe_2O_3.[29] In addition, the intensities of the absorption tails exhibit a gradual enhancement with the increased Co amounts, which can be ascribed to the progressive formation of oxygen vacancies.[42] Based on the above results, it is clearly demonstrated that the concentration of oxygen vacancies in α-Fe_2O_3 platelets can be significantly improved by Co decoration.

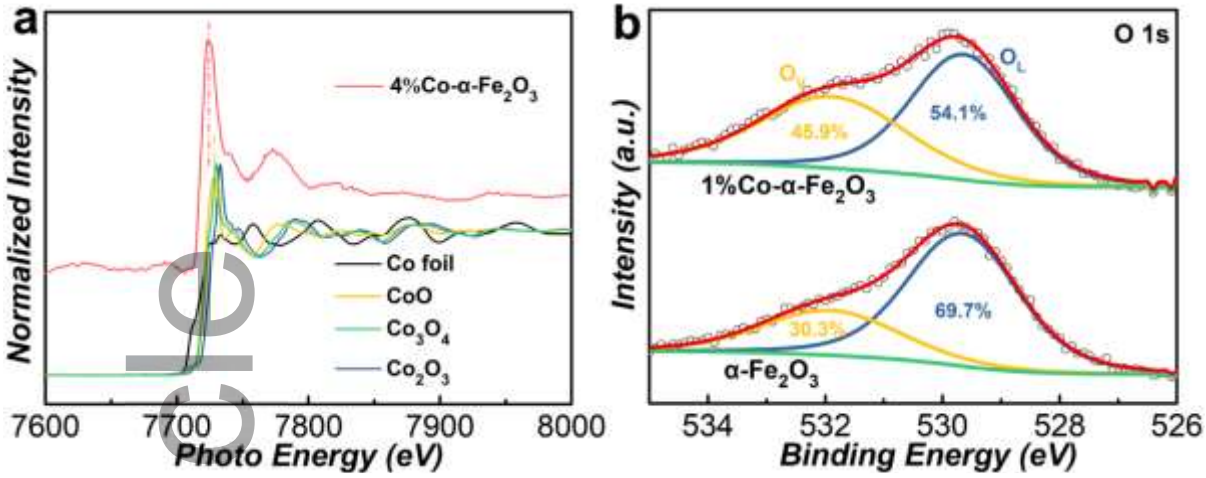

Figure 2. Structure characterizations. a) Co K-edge XANES spectra of 4%Co-α-Fe_2O_3 and references. b) O *1s* XPS spectra of α-Fe_2O_3 and 1%Co-α-Fe_2O_3.

To investigate the effects of confined Co sites and oxygen defects for α-Fe_2O_3 platelets, the photocatalytic performance for CO_2 reduction was measured with a tandem system, in which the $[Ru(bpy)_3]Cl_2$ (abbreviated as Ru) was utilized as the photosensitizer, triethanolamine (TEOA) was chose as the sacrificial agent (electron donor) and the as-prepared samples were served as the cocatalysts to capture the energetic electrons from photosensitizer. As presented in Figure 3a, although the photocatalytic performance of pure α-Fe_2O_3 is not so good (Figure 3a), it displays a much higher CO selectivity than the commercial α-Fe_2O_3 or FeOOH, indicating the unique feature of α-Fe_2O_3 platelets as support materials for photocatalytic CO_2 reduction. Remarkably, the introduction of confined Co centers on α-Fe_2O_3 platelets (1%Co-α-Fe_2O_3) drastically boosts the activity for CO_2 reduction, exhibiting a high CO generation rate of 37.8 μmol h^{-1} with an impressive selectivity of 80.2%, which is superior or comparable to the reported results with the similar photocatalytic systems (Table S2). This result clearly verifies that the decorated Co centers can proceed the catalytic processes efficiently as the reaction sites. It is notable that CO can be continuously generated in the initial 2.5 h, but its yield rate is gradually decreased with reaction prolonging (Figure S10). This phenomenon is commonly observed in the similar photocatalytic systems and should be ascribed to the degradation of the Ru photosensitizer.[8, 35] To further confirm the effect of confined Co centers, different metal sites were decorated on the α-Fe_2O_3 platelets to replace the Co sites (Figure S11), all of which display much lower photocatalytic performance for CO_2 reduction compared with the 1%Co-α-Fe_2O_3 (Figure 3b). In addition, the Co_{ion}-α-Fe_2O_3 prepared by direct absorption of Co^{2+} ions on α-Fe_2O_3 platelets displays poor performance compared with 1%Co-α-Fe_2O_3 (Figure S12). It is notable that the CO selectivity of the Co_{ion}-α-Fe_2O_3 (39.6%) is much lower than the 1%Co-α-Fe_2O_3 (80.2%), indicating that the confined Co centers in 1%Co-α-Fe_2O_3 is effective to inhibit the competing reaction of H_2 evolution during the photocatalytic CO_2 reduction. Therefore, the above results signify the extraordinary properties

of confined Co sites anchored on the α-Fe_2O_3 platelets for selective CO_2 photoreduction. Also, the 1%Co-α-Fe_2O_3 exhibits good recyclability for the photocatalytic reaction, with a stable selectivity and ~85% remained CO generation of its original value after five cycles (Figure S13). In addition, the structure and morphology are maintained and no content loss for the confined Co sites after the cycling (Figure S14), further verifying the durability of 1%Co-α-Fe_2O_3 for photocatalytic CO_2 reduction. However, as displayed in Figure 3a and Figure 3c, when further increasing the Co amount (more than 1%) on α-Fe_2O_3, although the photocatalytic activity would be slightly enhanced (with the similar CO selectivity), the turnover numbers (TON) display a huge decrease from 106.1 (1%Co-α-Fe_2O_3, 1 h) to 26.6 (4%Co-α-Fe_2O_3, 1 h). The low TON can be attributed to the agglomerated CoO_x nanoparticles with high loading amount, which is disclosed by the morphology and structure characterizations. Therefore, it can be confirmed that the utilization efficiency of Co atoms would be seriously suppressed if excessive Co species aggregate on the α-Fe_2O_3 support, further highlighting the importance of high dispersion for the active sites.

A series of control experiments were conducted under various conditions to identify the key factors for the CO_2 photoreduction system. As illustrated in Figure 3d, no product can be detected without the addition of Ru photosensitizer (the second column), indicating that independent 1%Co-α-Fe_2O_3 is inactive for the CO_2 photoreduction. Almost no CO is generated with the absence of catalysts (the first column), verifying that the bare Ru photosensitizer is hardly to trigger the CO_2 reduction. When the CO_2 reactant is replaced by the Ar (the third column), no generated CO is detected, manifesting that the CO product is indeed originated from the CO_2 feedstock. To verify this point, isotopic experiments labeled with $^{13}CO_2$ were conducted with the same photocatalytic conditions. As identified by the measurements of gas chromatography-mass spectrometry (Figure S15), the obtained product is assigned to the produced ^{13}CO, which can be the direct proof that the carbon source in the generated CO is originated from the CO_2 over the photocatalytic system.

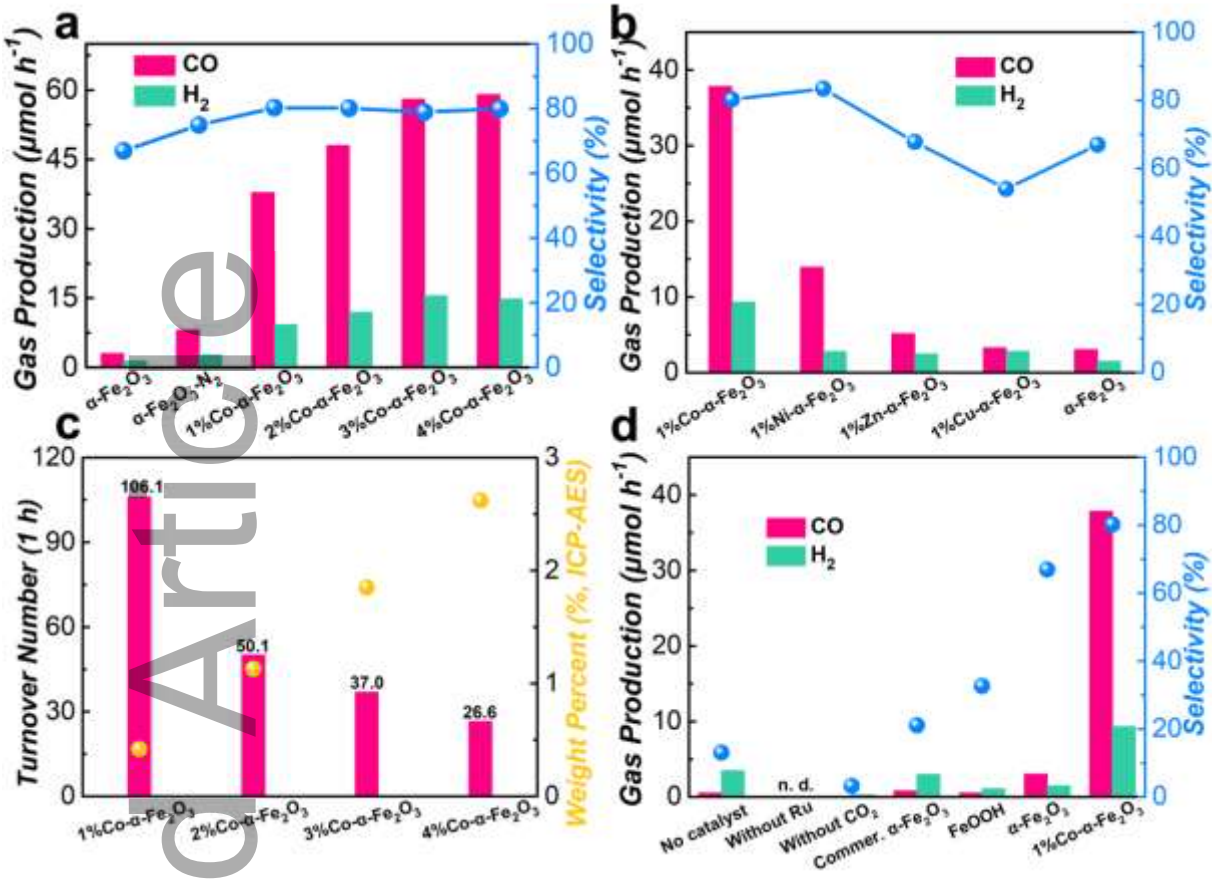

Figure 3. Measurements of CO_2 photoreduction performance. a) Comparison of CO_2 photoreduction activity with different cocatalysts. b) Activity comparison of α-Fe_2O_3 decorated with different metal centers. c) Turnover numbers of catalysts decorated with different loading amounts of Co species. d) Activity comparison of the catalytic system under different reaction conditions.

The crucial effects of the confined Co centers were verified by the measurements of photocatalytic performance in Figure 3. Then the role of the oxygen defects for photocatalytic CO_2 reduction was explored. Firstly, oxygen vacancies are intentionally introduced into the bare α-Fe_2O_3 via annealing in the N_2 (α-Fe_2O_3-N_2, Figure S17), which can be validated by the results in Figure S8, Figure S9b and Figure S16. Although the performance is much lower than that of the 1%Co-α-Fe_2O_3, the α-Fe_2O_3-N_2 still displays enhanced photocatalytic activity and selectivity compared with the pristine α-Fe_2O_3 (Figure 3a). Interestingly, the photocatalytic performance of the pristine α-Fe_2O_3 displays a distinct decrease after annealing in the air (Figure 4a), which is attributed to the diminished concentration of surface oxygen defects as determined by the XPS measurements (Figure 4b, Figure S18). Thus, it can be confirmed that the existence of oxygen defects is beneficial for photocatalytic CO_2 reduction. As verified by the CO_2 adsorption isotherms in Figure S20, the presence of oxygen defects can promote the ability for CO_2 adsorption, which may facilitate the stabilization of the key intermediates and thus promotes the CO_2 reduction.[29] Subsequently, the influence of oxygen defects on the confined Co centers was further investigated. As

shown in Figure 4c-4d, both of the activity and selectivity exhibit huge decreases for 1%Co-α-Fe_2O_3 after annealing in the air owing to the reduced oxygen defects. This phenomenon can be the direct proof of the synergetic effect between confined Co centers and oxygen defects for CO_2 photoreduction. Therefore, it can be deduced that although the intrinsic catalytic activity of oxygen defects in α-Fe_2O_3 is moderate, the oxygen defects can significantly promote the catalytic activity of confined Co active sites when work cooperatively due to the improved CO_2 adsorption. However, it should be noted that the photocatalytic performance of 1%Co-α-Fe_2O_3-N_2 only displays a slight enhancement compared with the 1%Co-α-Fe_2O_3 (Figure S21). Owing to the significant influence of Co decoration, the annealing treatment would have weak effects for the generation of oxygen defects after Co decoration for 1%Co-α-Fe_2O_3, as verified by the O *1s* XPS spectrum of 1%Co-α-Fe_2O_3-N_2 in Figure S22 (the ratio for oxygen defects varied from 45.9% to 47.4% after annealing in the N_2).

Figure 4. a-b) Comparison of activity and O *1s* XPS spectra between α-Fe_2O_3 and α-Fe_2O_3-air (α-Fe_2O_3 annealed in the air). c-d) Comparison of activity and O *1s* XPS spectra between 1%Co-α-Fe_2O_3 and 1%Co-α-Fe_2O_3-air (1%Co-α-Fe_2O_3 annealed in the air).

The charge carrier dynamics of different catalysts was also elucidated. Firstly, the photoluminescence (PL) spectroscopy was utilized to probe the recombination of the photogenerated carriers. As shown in

Figure 5a, the emission of Ru photosensitizer is quenched when the as-prepared cocatalysts are introduced, indicating the recombination of photogenerated charge carriers has been substantially suppressed.[43] In addition, the existence of confined Co sites and oxygen defects can further restrict the charge recombination by acting as the trapping sites for the photogenerated carriers, as presented with the lower PL intensities of α-Fe_2O_3-N_2 and 1%Co-α-Fe_2O_3 compared with the pure α-Fe_2O_3. Subsequently, time-resolved transient photoluminescence delay (TRPL) measurement was carried out to experimentally investigate the charge behaviors of the photocatalytic system.[44] As displayed in Figure 5b and Table S1, the Ru photosensitizer exhibits a long average lifetime of 406.8 ns, which is similar to the reported results.[43] The introduction of cocatalysts can significantly reduce the average lifetimes. The 1%Co-α-Fe_2O_3 exhibits a shorter lifetime (219.9 ns) than α-Fe_2O_3-N_2 (252.0 ns) and pure α-Fe_2O_3 (309.7 ns), verifying the greatly enhanced charge transfer induced by the synergy of confined Co sites and oxygen defects. Based on the above results, the relevant photocatalytic processes for CO_2 reduction are demonstrated in Figure 5d. Upon irradiating by the visible light, energetic electrons can be excited from the Ru photosensitizer and transferred to the confined Co centers on the α-Fe_2O_3 platelets, where CO_2 molecule is activated and reduced to CO. Simultaneously, the oxidized Ru photosensitizer would be reduced by the sacrificial reductant TEOA to form an entire cycle.

Density functional theory (DFT) calculation was utilized to explore the origin of the synergistic effects between confined Co sites and oxygen defects for superior photocatalytic CO_2 reduction (Figure S23). Generally, the first step of the CO_2 conversion is the adsorption of CO_2 molecules onto the catalysts ($CO_2 \rightarrow CO_2^*$).[45, 46] Therefore, in order to verify the effects of oxygen defects for CO_2 adsorption, the adsorption energy of CO_2 molecule on bare α-Fe_2O_3 and α-Fe_2O_3 with oxygen vacancies (α-Fe_2O_3-N_2) were calculated, respectively. As shown in Figure 5c, the adsorption energy of CO_2 on α-Fe_2O_3-N_2 (-0.40 eV) is stronger than that of the bare α-Fe_2O_3 (-0.27 eV), implying the enhanced adsorption affinity of oxygen defects towards CO_2. In addition, the synergy of confined Co centers and oxygen defects (1%Co-α-Fe_2O_3) can further improve the CO_2 adsorption energy to -0.86 eV, which is consistent with the experimental measurements in Figure S17.[47] The stronger CO_2 adsorption energy can stabilize the key intermediates and thus proceed the CO_2 reduction more smoothly.[48] After CO_2 adsorption onto the catalysts, the photocatalytic conversion from CO_2 to CO generally undergo the pathways of $COOH^*$, CO^* and CO in order.[7] To further understanding the catalytic processes of different catalysts, the free energy for every step was also calculated and displayed in Figure 5c. The energy barrier is the minimum amount of energy that must be provided to complete the relevant chemical reaction, which is indicated in Figure 5c for CO_2 reduction with different catalysts. The calculated results disclose that the activation energy barrier for CO generation over 1%Co-α-Fe_2O_3 (1.28 eV) is smaller than that of α-Fe_2O_3 with only oxygen defects (α-Fe_2O_3-

N_2, 1.77 eV) and pristine α-Fe_2O_3 (1.79 eV), indicating that the synergy of confined Co centers and oxygen defects is kinetically more favorable for the formation of CO with CO_2 reduction.

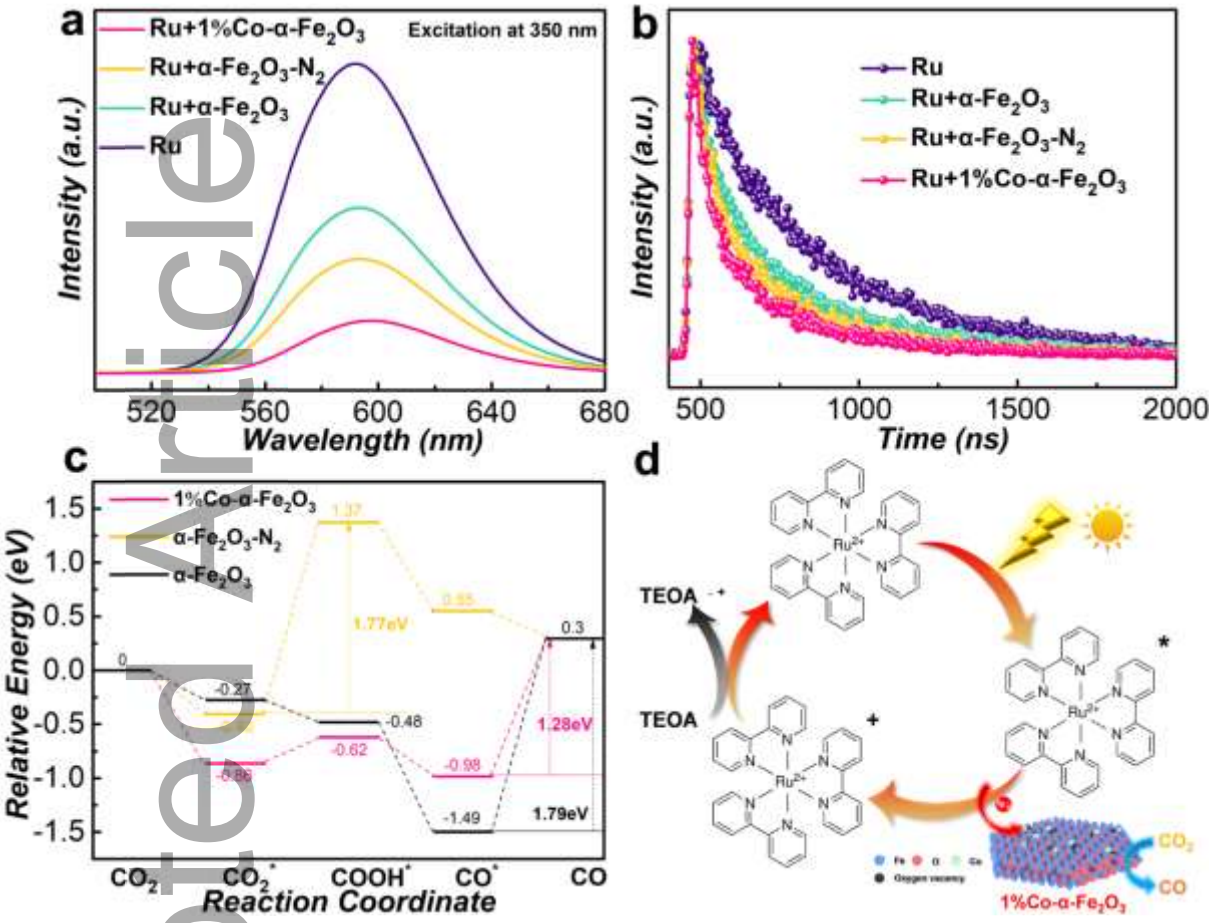

Figure 5. a) Steady-state PL spectra and b) time-resolved PL spectra of different samples. c) Calculated free energy of CO_2 reduction reaction with different catalysts. d) Scheme of the photocatalytic processes for CO_2 reduction.

3. Conclusion

In this study, we demonstrate a synergetic effect between confined Co centers and oxygen defects on α-Fe_2O_3 platelets for efficient photocatalytic CO_2 reduction. The highly dispersed Co sites are spontaneously confined into the α-Fe_2O_3 platelets during the preparation processes and abundant oxygen defects are generated simultaneously along with the Co decoration. Experimental results and theoretical calculations verify that the confined Co sites not only perform as the active centers for CO_2 conversion but also significantly facilitate the transfer of energetic electrons from the photosensitizer, while the oxygen vacancies can enhance the adsorption ability for CO_2 molecules. When combining together, the oxygen defects can fundamentally promote the CO_2 reduction capability of confined Co sites, resulting in greatly accelerated catalytic kinetics and enhanced efficiency for CO_2 photoreduction. This work may offer new

opportunities to design novel catalysts that combining robust active sites and defect engineering for efficient solar-driven photocatalysis.

Supporting Information

Supporting Information is available from the Wiley Online Library or from the author.

Acknowledgements

This work received financial support from the World Premier International Research Center Initiative (WPI Initiative) on Materials Nanoarchitectonics (MANA), MEXT (Japan), JSPS KAKENHI (JP18H02065), the Photo-excitonix Project at Hokkaido University, National Natural Science Foundation of China (21633004, 22001094), the Fellowship of China Postdoctoral Science Foundation (2020M673057, 2020TQ0123) and Guangdong Basic and Applied Basic Research Foundation (2020A1515110003). We thank Dr. Shengyao Wang and Dr. Huiwen Lin for their constructive suggestions and great support.

Received: ((will be filled in by the editorial staff))
Revised: ((will be filled in by the editorial staff))
Published online: ((will be filled in by the editorial staff))

References

[1] H. Tong, S. Ouyang, Y. Bi, N. Umezawa, M. Oshikiri, J. Ye, *Adv. Mater.* **2012,** *24*, 229-251.

[2] X. Li, J. Yu, M. Jaroniec, X. Chen, *Chem. Rev.* **2019,** *119*, 3962-4179.

[3] J. L. White, M. F. Baruch, J. E. Pander, Y. Hu, I. C. Fortmeyer, J. E. Park, T. Zhang, K. Liao, J. Gu, Y. Yan, T. W. Shaw, E. Abelev, A. B. Bocarsly, *Chem. Rev.* **2015,** *115*, 12888-12935.

[4] J. Ran, M. Jaroniec, S.-Z. Qiao, *Adv. Mater.* **2018,** *30*, 1704649.

[5] W. Tu, Y. Zhou, Z. Zou, *Adv. Mater.* **2014,** *26*, 4607-4626.

[6] L. Liu, Y. Zhang, H. Huang, *Solar RRL* **2021,** *5*, 2000430.

[7] Y. Li, S. Wang, X.-S. Wang, Y. He, Q. Wang, Y. Li, M. Li, G. Yang, J. Yi, H. Lin, D. Huang, L. Li, H. Chen, J. Ye, *J. Am. Chem. Soc.* **2020,** *142*, 19259-19267.

[8] H. Zhang, Y. Wang, S. Zuo, W. Zhou, J. Zhang, X. W. D. Lou, *J. Am. Chem. Soc.* **2021,** *143*, 2173-2177.

[9] X.-S. Wang, L. Li, D. Li, J. Ye, *Solar RRL* **2020,** *4*, 1900547.

[10] S. Zhong, Y. Xi, S. Wu, Q. Liu, L. Zhao, S. Bai, *J. Mater. Chem. A* **2020,** *8*, 14863-14894.

[11] Q. Guo, X. Feng, Z. C. Zhang, L. Huang, *Solar RRL* **2021,** *5*, 2100234.

[12] W. Chen, X. Liu, B. Han, S. Liang, H. Deng, Z. Lin, *Nano Res.* **2021**, *14*, 730-737.

[13] Y. Wang, S. Wang, X. W. Lou, *Angew. Chem. Int. Ed.* **2019**, *58*, 17236-17240.

[14] K.-Q. Lu, Y.-H. Li, F. Zhang, M.-Y. Qi, X. Chen, Z.-R. Tang, Y. M. A. Yamada, M. Anpo, M. Conte, Y.-J. Xu, *Nat. Commun.* **2020,** *11*, 5181.

[15] Y. Shi, M. Li, Y. Yu, B. Zhang, *Energy Environ. Sci.* **2020,** *13*, 4564-4582.

[16] S. Wang, B. Y. Guan, Y. Lu, X. W. D. Lou, *J. Am. Chem. Soc.* **2017,** *139*, 17305-17308.

[17] S. Wang, Z. Ding, X. Wang, *Chem. Commun.* **2015**, *51*, 1517-1519.

[18] H. B. Yang, S.-F. Hung, S. Liu, K. Yuan, S. Miao, L. Zhang, X. Huang, H.-Y. Wang, W. Cai, R. Chen, J. Gao, X. Yang, W. Chen, Y. Huang, H. M. Chen, C. M. Li, T. Zhang, B. Liu, *Nat. Energy* **2018,** *3*, 140-147.

[19] A. Wang, J. Li, T. Zhang, *Nat. Rev. Chem.* **2018,** *2*, 65-81.

[20] H. Rao, L. C. Schmidt, J. Bonin, M. Robert, *Nature* **2017,** *548*, 74-77.

[21] X.-F. Yang, A. Wang, B. Qiao, J. Li, J. Liu, T. Zhang, *Acc. Chem. Res.* **2013,** *46*, 1740-1748.

[22] C. Gao, J. Low, R. Long, T. Kong, J. Zhu, Y. Xiong, *Chem. Rev.* **2020,** *120*, 12175-12216.

[23] H. Zhang, G. Liu, L. Shi, J. Ye, *Adv. Energy Mater.* **2018,** *8*, 1701343.

[24] C. Gao, S. Chen, Y. Wang, J. Wang, X. Zheng, J. Zhu, L. Song, W. Zhang, Y. Xiong, *Adv. Mater.* **2018,** *30*, 1704624.

[25] P. Huang, J. Huang, S. A. Pantovich, A. D. Carl, T. G. Fenton, C. A. Caputo, R. L. Grimm, A. I. Frenkel, G. Li, *J. Am. Chem. Soc.* **2018,** *140*, 16042-16047.

[26] S. Ji, Y. Chen, X. Wang, Z. Zhang, D. Wang, Y. Li, *Chem. Rev.* **2020,** *120*, 11900-11955.

[27] S. Wang, W. Yao, J. Lin, Z. Ding, X. Wang, *Angew. Chem. Int. Ed.* **2014,** *53*, 1034-1038.

[28] L. Zhang, X. Zhao, Z. Yuan, M. Wu, H. Zhou, *J. Mater. Chem. A* **2021,** *9*, 3855-3879.

[29] J. Wu, X. Li, W. Shi, P. Ling, Y. Sun, X. Jiao, S. Gao, L. Liang, J. Xu, W. Yan, C. Wang, Y. Xie, *Angew. Chem. Int. Ed.* **2018,** *57*, 8719-8723.

[30] L. Ran, J. Hou, S. Cao, Z. Li, Y. Zhang, Y. Wu, B. Zhang, P. Zhai, L. Sun, *Solar RRL* **2020,** *4*, 1900487.

[31] J. Zhang, R. Yin, Q. Shao, T. Zhu, X. Huang, *Angew. Chem. Int. Ed.* **2019,** *58*, 5609-5613.

[32] L. Wang, G. Liu, B. Wang, X. Chen, C. Wang, Z. Lin, J. Xia, H. Li, *Solar RRL* **2021,** *5*, 2000480.

[33] M. Xiao, L. Zhang, B. Luo, M. Lyu, Z. Wang, H. Huang, S. Wang, A. Du, L. Wang, *Angew. Chem. Int. Ed.* **2020,** *59*, 7230-7234.

[34] Y. Xue, B. Huang, Y. Yi, Y. Guo, Z. Zuo, Y. Li, Z. Jia, H. Liu, Y. Li, *Nat. Commun.* **2018,** *9*, 1460.

[35] C. Gao, Q. Meng, K. Zhao, H. Yin, D. Wang, J. Guo, S. Zhao, L. Chang, M. He, Q. Li, H. Zhao, X. Huang, Y. Gao, Z. Tang, *Adv. Mater.* **2016,** *28*, 6485-6490.

[36] A. Bergmann, E. Martinez-Moreno, D. Teschner, P. Chernev, M. Gliech, J. F. de Araújo, T. Reier, H. Dau, P. Strasser, *Nat. Commun.* **2015,** *6*, 8625.

[37] J. Yan, L. Kong, Y. Ji, J. White, Y. Li, J. Zhang, P. An, S. Liu, S.-T. Lee, T. Ma, *Nat. Commun.* **2019,** *10*, 2149.

[38] Z. Wang, X. Mao, P. Chen, M. Xiao, S. A. Monny, S. Wang, M. Konarova, A. Du, L. Wang, *Angew. Chem. Int. Ed.* **2019,** *58*, 1030-1034.

[39] G. Yang, Y. Li, H. Lin, X. Ren, D. Philo, Q. Wang, Y. He, F. Ichihara, S. Luo, S. Wang, J. Ye, *Small Methods* **2020,** *4*, 2000577.

[40] Y. Lv, Y. Liu, Y. Zhu, Y. Zhu, *J. Mater. Chem. A* **2014,** *2*, 1174-1182.

[41] S. Wang, X. Hai, X. Ding, K. Chang, Y. Xiang, X. Meng, Z. Yang, H. Chen, J. Ye, *Adv. Mater.* **2017,** *29*, 1701774.

[42] H. Yu, J. Li, Y. Zhang, S. Yang, K. Han, F. Dong, T. Ma, H. Huang, *Angew. Chem. Int. Ed.* **2019,** *58*, 3880-3884.

[43] J. Yang, Z. Wang, J. Jiang, W. Chen, F. Liao, X. Ge, X. Zhou, M. Chen, R. Li, Z. Xue, G. Wang, X. Duan, G. Zhang, Y.-G. Wang, Y. Wu, *Nano Energy* **2020,** *76*, 105059.

[44] L. Shi, P. Wang, Q. Wang, X. Ren, F. Ichihara, W. Zhou, H. Zhang, Y. Izumi, B. Cao, S. Wang, H. Chen, J. Ye, *J. Mater. Chem. A* **2020,** *8*, 21833-21841.

[45] Z. Sun, T. Ma, H. Tao, Q. Fan, B. Han, *Chem* **2017,** *3*, 560-587.

[46] B. Han, X. Ou, Z. Deng, Y. Song, C. Tian, H. Deng, Y.-J. Xu, Z. Lin, *Angew. Chem. Int. Ed.* **2018,** *57*, 16811-16815.

[47] Z. Geng, X. Kong, W. Chen, H. Su, Y. Liu, F. Cai, G. Wang, J. Zeng, *Angew. Chem. Int. Ed.* **2018,** *57*, 6054-6059.

[48] Y. Wang, N.-Y. Huang, J.-Q. Shen, P.-Q. Liao, X.-M. Chen, J.-P. Zhang, *J. Am. Chem. Soc.* **2018,** *140*, 38-41.

This study demonstrates a synergetic effect between confined Co centers and oxygen defects on α-Fe_2O_3 platelets for efficient photocatalytic CO_2 reduction. The oxygen defects can fundamentally promote the catalytic capability of the confined Co sites, resulting in greatly accelerated charge transfer and reduced energy barriers for CO_2 photoreduction.

Gaoliang Yang, Yunxiang Li, Qi Wang, Xusheng Wang,* Shouwei Zuo, Huabin Zhang, Xiaohui Ren, Yu He, Fumihiko Ichihara and Jinhua Ye*

Synergy between Confined Cobalt Centers and Oxygen Defects on α-Fe_2O_3 Platelets for Efficient Photocatalytic CO_2 Reduction